Molecular Catalysis 486 (2020) 110833

Contents lists available at ScienceDirect

Molecular Catalysis

journal homepage: www.elsevier.com/locate/mcat

Zn-promoted Hβ zeolite for gas-phase catalyzed aza-heterocyclic-aromatization of acrolein dimethyl acetal and aniline to quinolines

An Li[a,*,1], Caiwu Luo[b,1], Yong Liu[b], Lijun Li[a], Ying Lin[a], Kun Liu[a,*], Congshan Zhou[a,*]

[a] College of Chemistry and Chemical Engineering, Hunan Institute of Science and Technology, Yueyang, Hunan, 414000, China
[b] Hunan Province Engineering Research Center of Radioactive Control Technology in Uranium Mining and Metallurgy & Hunan Province Engineering Technology Research Center of Uranium Tailings Treatment Technology, and Cooperative Innovation Center for Nuclear Fuel Cycle Technology and Equipment, University of South China, Hengyang 421001, China

ARTICLE INFO

Keywords:
Zn-promoted
Vapor-phase
Aza-heterocyclic
Acrolein diethyl acetal
Quinolines

ABSTRACT

Catalytic activities of Zn-promoted Hβ zeolite for gas-phase aza-heterocyclic-aromatization of acrolein dimethyl acetal and aniline to quinolines were investigated. the Zn/Hβ catalyst showed better selectivity to quinoline than the parent Hβ one. Characterization results demonstrated that the Zn/Hβ catalyst prepared via deposition precipitation method existed the isolated Zn^{2+} cations as well as the highly dispersed ZnO clusters, which not only decreased concentration of strong acid sites but also enhanced enhance aromatization process. As a result, the decrease of strong acid sites restrained the cracking of acrolein to acetaldehyde as well as the alkylation of quinoline to ethylquinoline effectively; and the Zn species of catalyst further improved aromatization process of dihydroquinoline to quinoline. Moreover, the Zn/Hβ catalyst presented relatively enhanced ability of anti-activation and excellent regenerability, owing to decrease strong acid-induced polymerization of active intermediates to form the coking. Under the optimized operating conditions, more than 51 % yield of quinoline was achieved over Zn/Hβ catalyst; which far exceeded quinoline yield (28 %) over the pure Hβ one. Besides, a plausible reaction routes in vapor-phase acrolein diethyl acetal with aniline to quinolines were suggested in this paper.

1. Introduction

Aza-heterocyclic compounds exhibit excellent therapeutic and biological properties, which are abundant in a great variety of synthetic drugs and natural products [1–5]. Particularly, quinoline and quinoline derivatives, as an important category of aza-heterocyclic compounds, present attractive pharmacological activities for new drug development [4,5]. Among the aza-heterocycles synthetic methods, C-heteroatom bond forming cascade reactions are usually utilized to build versatile aza-heterocyclic skeletons [6,7]; and especially, Doebner-Von Miller condensation is considered one of the most useful aza-heterocyclic synthetic routes to generate quinolines skeletons via aza-heterocyclic-aromatization processes [8–10].

The typical Doebner-Von Miller condensation to quinolines was conducted via conventional batch-type liquid-phase condition. Meanwhile, homogeneous catalysts were usually employed, such as, hydrochloric acid, sulfuric acid or acid minerals [8,9,11–13]. As a result, the batch-type liquid-phase process suffers from several disadvantages of toxic and volatile organic solvents and complicated catalysts separation, which is not helpful for the eco-friendly and mass production of quinolines. Unlike the conventional liquid-phase approach, continuous gas-phase method has numerous advantages of continuous production, absent acid stream, convenient product recovery and simplified catalyst regenerability, showing more and more potential for the production of quinolines at present [14–18]. In addition, saturated/unsaturated aldehydes or ketones, such as acrolein, formaldehyde, acetaldehyde, and butenal, were preferred feedstocks to be employed in the Doebner-Von Miller reaction. However, those feedstocks come from fossil resources (nocuous, non-renewable and costly) and easily cause polymerization themselves under gas-phase process (probably leading to serious catalyst deactivation) [14,16]. Alternatively, acrolein acetals shows attractive chemical stability, excellent diffusion ability and carbonyl protection, which could be obtained with excellent selectivity and high yield by means of aldehydes/ketones directly reacting with alcohols [19–21]. As a consequence, the employment of acrolein acetals to replace saturated/unsaturated

* Corresponding authors.
E-mail addresses: anleechn@hotmail.com (A. Li), liukun328@126.com (K. Liu), zhoucongsh@126.com (C. Zhou).
[1] Coauthors equally contributed to this work.

https://doi.org/10.1016/j.mcat.2020.110833
Received 18 November 2019; Received in revised form 6 February 2020; Accepted 6 February 2020

aldehydes or ketones as one of feedstocks to generate quinolines is a good strategy [20,21], which could not only distinctly overcome aldehydes/ketones's relatively high cost but also retard the polymerization at relative high reaction temperature. Hence, the further development of gas-phase aza-heterocyclic-aromatization from acrolein acetals and aniline to quinolines is of great interest and highly necessitated.

Zn species supported on zeolites have been extensively applied in different types of reactions, containing alkane methanol-to-formaldehyde [22], waste water treatment [23], photocatalytic degradation [24,25], hydrogenation and dehydrogenation [26,27]. Especially, Zn species possess excellent catalytic performance of aromatization, due to its more superior ability of leaching hydrogen from subtracts compared to other traditional transition metal counterparts [28–30]. Hβ-typed zeolites, presenting three-dimensional structure with 12-ring channel systems, have been considerably explored as catalyst for the vapor-phase synthesis of quinolones [14,31,32]. Compared to others catalysts [16,17,33–35], such as mixed metal oxides, amorphous silica-alumina, modified-montmorillonite and halide clusters, the Hβ zeolites possesses numerous obvious merits, involving high surface area, excellent stability of thermal and hydrothermal, shape selectivity, low coke formation, adjustable acidity and appropriate microporous size matching with bulky quinolines molecule size [36–38]. It is reported that Hβ zeolite-base catalysts were effective catalysts for synthesis of quinolines from various raw materials involving acetaldehyde [14], glycerol [31], lactic acid [32], and formaldehyde [39]. For example, Roald Brosius employed the Hβ zeolite and F-modified Hβ as catalysts to vapor-phase synthesis quinolines from aniline and acetaldehyde; and more than 83 % sum totals of quinolines (including quinoline, 2-methylquinoline and 4-methylquinoline) were obtained [14]. When the Hβ zeolite combined with Zn species, the catalytic activity of the Zn/Hβ system could be significantly improved; because the addition of Zn species into zeolite could regulate concentration and strength of acidity of catalyst effectively. Moreover, Zn species itself can play determining active sites in aromatization, which is necessary process in the reaction of acrolein acetals and aniline to quinolones [40]. To the best of our knowledge, little literatures known so far for the gas-phase catalyzed aza-heterocyclic-aromatization to quinolines over Zn-modified Hβ zeolite catalysts was shown in detail.

In the present paper, the Zn-modified Hβ catalysts were prepared via deposition precipitation and employed in the gas-phase aza-heterocyclic-aromatization of aniline and acrolein dimethyl acetal to quinolines. Reaction conditions, activity, stability as well as regeneration of catalysts were systematically investigated. The influence of Zn-supported on zeolites for the activity and selectivity is addressed. Meanwhile, a feasible vapor-phase reaction pathway was suggested in this paper.

2. Experimental

2.1. Chemicals

The parent β zeolite was purchased from Nankai University Catalyst Factory. Urea, zinc nitrate and other metal salts were purchased from Xilong Chemical Company. Acrolein diethyl acetal, aniline and ethanol were supplied by Sinopharm Chemical Reagent Company.

2.2. Catalyst preparation

2.2.1. H-typed β zeolite catalyst prepared via ion-exchange

The ion-exchange method was used to prepare H-typed β zeolite. Firstly, the parent β zeolite powder was added into 1.0 M NH_4NO_3 solution to form suspension, and then refluxed at 90 °C for 4 h under vigorous stirring. Following by filtrated, washed with distilled water and dried sufficiently at 120 °C, the NH_4-typed β zeolite powder was obtained. The above processes were repetitively operated three times. Finally, the dried NH_4-typed β zeolite powder was calcined at 550 °C for 4 h, and the thus-obtained catalyst was named as Hβ.

2.2.2. Zn/Hβ zeolite catalyst prepared via deposition precipitation

The Zn-modified β zeolite catalyst was prepared via deposition precipitation. Firstly, a homogeneous aqueous solution was prepared by the mixture of zinc nitrate, urea and deionized water; and then, the prepared Hβ zeolite powder was added to form the suspension. Subsequently, the suspension was vigorously stirred under room temperature for 2 h and then heated to 90 °C for refluxing 4 h. After cooling down, the suspension was treated by filtrating, washing, and drying completely. Finally, the obtained solid powder was calcined at 550 °C for 4 h, named as Zn/Hβ.

As comparison, other metal-supported Hβ zeolite catalysts were also prepared according to the above method, using corresponding nitrates as the precursors, which named as M/Hβ (M = Cr- Ni- Mn- Cu- and Fe). The P- and F-supported Hβ zeolite catalysts were prepared via impregnation method as follow: the homogeneous precursor solution of $(NH_4)_2HPO_4$ or NH_4F was firstly prepared, and then the Hβ zeolite powder was added and continuous stirred for 6 h under room temperature. Follow by filtrating, washing, and drying completely, the obtained solid powder was calcined at 550 °C for 4 h, and the thus-prepared catalysts were denoted as P/Hβ and F/Hβ respectively.

2.3. Catalysts characterization

X-ray diffraction patterns (XRD) for catalysts were performed on Bruker D8 diffractometer, Cu-Kα radiation (λ = 1.54187 Å). Fourier transform infrared (FT-IR) spectroscopy were recorded on a Varian 3100 spectrometer using the GTGS detector under resolution of 2 cm^{-1} and scanning number of 32. Scanning electron microscopy (SEM) was performed on a JEOL JSM 6700 F at an accelerating voltage of −5.0 kV. Transmission Electron Microscope (TEM) was carried out with a JEM-2100 F equipment with an accelerating voltage of 200 kV. Before measurement, the sample was ultrasonic treated in order to disperse the sample powder in ethanol, and then dropped onto a carbon-coated copper grid. High-Resolution Transmission Electron Microscopy (HRTEM) was made with a JEM-2200FS microscope. The Hβ and Zn/Hβ catalyst samples were firstly suspended in ethanol and then deposited on carbon-film-coated copper grids. N_2 adsorption-desorption isothermal were measured on a Quantachrome Autosorb-1 analyzer at 77 K; all the catalysts were initially degassed at 300 °C in a vacuum condition of 10^{-8} Torr for 12 h before measurement. Temperature-programmed desorption of ammonia (NH_3-TPD) was conducted on an Autochem II 2920 instrument. Typically, all the catalysts were firstly pretreated in He flow (60 ml/min) for 0.5 h at 400 °C before NH_3 adsorption, and then 10 vol. % NH_3 in He (50 ml/min) was adsorbed to reach saturation over catalyst. Subsequently, the physically adsorbed NH_3 was purged in a flow of helium at 100 °C, and then ammonia was desorbed from 100 to 800 °C with the heating rate of 10 °C/min. X-ray photoelectron spectroscopy (XPS) were carried out a PHI Quantum 2000 instrument with Al Ka radiation source. The suitable amount catalyst was compressed into a wafer for analysis. The signal of carbon C 1 s was present at 284.6 eV. Thermogravimetry (TG) were measured on a Diamond instrument; the deactivated catalysts were heated from room temperature to 800 °C in air (30 mL/min) with the heating rate of 5 °C/min.

2.4. Catalytic performance evaluation

The gas-phase reaction was conducted in a fixed-bed reactor. Firstly, the catalyst was filled in the middle of the stainless steel reaction tube. The reactor was heating to reaction temperature with a flow of nitrogen. Later on, feedstocks were initially vapored and subsequently fed into the reaction tube. The reaction was carried out under different reaction conditions, and the product mixtures were collected via cooling with ice-water trap. The product mixtures were identified by

means of Varian Saturn 2200/CP-3800 chromatography-mass spectrometry equipped with two CP8944 capillary columns (VF-5, 30 m ×0.25 mm ×0.25 μm). The yield of quinolines (containing quinoline (Q), methylquinoline(MeQ) and ethylquinoline(EtQ) was calculated on the basis of the converted acrolein diethyl acetal(ADA).

$$\text{Conversion (mol\%)} = \frac{\text{moles of ADA converted}}{\text{moles of ADA input}} \times\%$$

$$\text{Selectivity (mol\%)} = \frac{\text{moles of product}}{\text{moles of ADA converted}} \times\%$$

$$\text{Yield (mol\%)} = \text{Conversion} \times \text{Selectivity} \times\%$$

3. Results and discussions

3.1. Catalytic activity

The gas-phase reaction of ADA and aniline to Q undergoes two steps, involving hydrolysis of ADA to acrolein and next condensation of aniline and acrolein to quinoline [11]. In this reaction, besides quinolines (Q, MeQ and EtQ), byproducts (such as acetaldehyde, alkylaniline, methylindole and dimethylindol) are also generated and identified via mass spectrometry. The results of catalytic performance are shown as follow:

Fig. 1(a) showed the effect of nonmetal/metal-modified Hβ catalysts, in which the load amount of nonmetal/metal on Hβ was 5 wt%. Compared to Hβ catalyst, the yield of Q and Q_s decreases distinctly over the F- and P-supported Hβ ones, whereas that of Q_s declines in different degrees but that of Q increases observably over Cr-, Ni-, Mn-, Cu-, Fe- and Zn-supported Hβ ones. Moreover, the ratio of Q/Q_s increases significantly over metal-supported Hβ catalyst. Particularly, the yield of Q increases sharply to 51 % over the Zn/Hβ one. In addition, the effect of Zn loading is also performed, as shown in Fig. 1(b). The yield of MeQ and EtQ decreases with increasing Zn loading amount. By contrast, the yield of Q increases slightly initially and then decreases gradually, arriving the maximum yield of Q with 5 wt.% loading amount of Zn, indicating that an appropriate amount of Zn species on zeolite could promote the generation of Q more effectively.

Those above results reflect that nonmetal/metal-modification for Hβ zeolite significantly affects catalytic activity to quinolines in this reaction. It is reported that weak acid sites favor the generation of Q [31], while strong acid sites could promote cracking of acrolein to acetaldehyde and the alkylation of Q with ethanol to alkylquinolines [35,41]. When F and P species was supported on Hβ zeolite using $(NH_4)_2HPO_4$ or NH_4F as precursor, the concentration of strong acid sites over F/Hβ and P/Hβ catalysts should change little over F/Hβ and P/Hβ catalysts relative to the parent Hβ one. Because the NH_4^+ exchanged on zeolite could be re-converted to H^+ and the strong acid sites are recovered after calcining at high temperature. Thereby, there is no obvious improvement in quinolines synthetic reaction over the F/Hβ and P/Hβ catalysts. When metal species was supported on Hβ zeolite, from NH_3-TPD results (see Fig. 1S and Table 1S), one can see that metal modification on Hβ zeolite greatly reduces the concentration of strong Brønsted acid sites of catalyst; and particularly, the Zn/Hβ catalyst presents the least concentration of strong acid sites among all the metal-modified Hβ catalysts. From XPS result (see Fig. 9), one can see that the Zn/Hβ catalyst not only exists the isolated Zn^{2+} cations to decrease concentration of strong acid sites, but also exists the highly dispersed ZnO clusters to enhance the dehydrogenation to aromatization [26,27]. As a result, the metal-modified Hβ catalysts are able to retard the cracking and alkylation process effectively and then facilitate the condensation process of aniline and acrolein; and especially, the Zn/Hβ catalyst could promote the aromatization process of dihydroquinoline to Q (see Scheme 1). Thus, the Zn-modified Hβ one possesses more excellent catalytic activity to Q, compared to Cr-, Ni-, Mn-, Cu- and Fe-modified Hβ catalysts. From the above results, it could be concluded that the Zn^{2+} cations together with dispersed ZnO clusters over Zn/Hβ catalyst plays the multiple action in catalyzing aza-heterocyclic-aromatization of acrolein dimethyl acetal and aniline to quinolones.

Fig. 2 shows the effect of reaction conditions over Zn/Hβ catalyst, including temperature, molar ratio of AN/ADA, liquid hourly space velocity (LHSV) of mixture feedstocks as well as LHSV of H_2O. These reactions have been carried out on the basis of condition gradual optimization, and the results are shown as follows:

(1) Temperature. As shown in Fig. 2(a), the total yield increase obviously reaching ca. 75 % as its maximum with elevating temperature from 380 to 410 °C, and then decreases obviously. Similarly, yield of Q increases with elevating reaction temperature, obtaining its maximums of 51 % at 440 °C, and then decreases obviously. This occurs mainly due that, reaction temperature at the range of 400 − 500 °C favors the formation of quinolines [14,42]. However, an excessively higher reaction temperature facilitates deep cracking of ADA and/or polymerization of intermediate acrolein, leading to the rapid decreasing of yield of quinolines. Therefore, the optimized temperature is selected at 440 °C based on the maximum yield of quinoline in this reaction.

(2) Ratio of AN/ADA. As shown in Fig. 2(b), yield of Q_s as well as Q increases with elevating molar ratio of AN/ADA, arriving its maximum at ratio of AN/ADA = 3, respectively, and then decrease to some extent. In this reaction, Q is generated undergoing the hydrolysis of ADA to acrolein/ethanol and subsequently

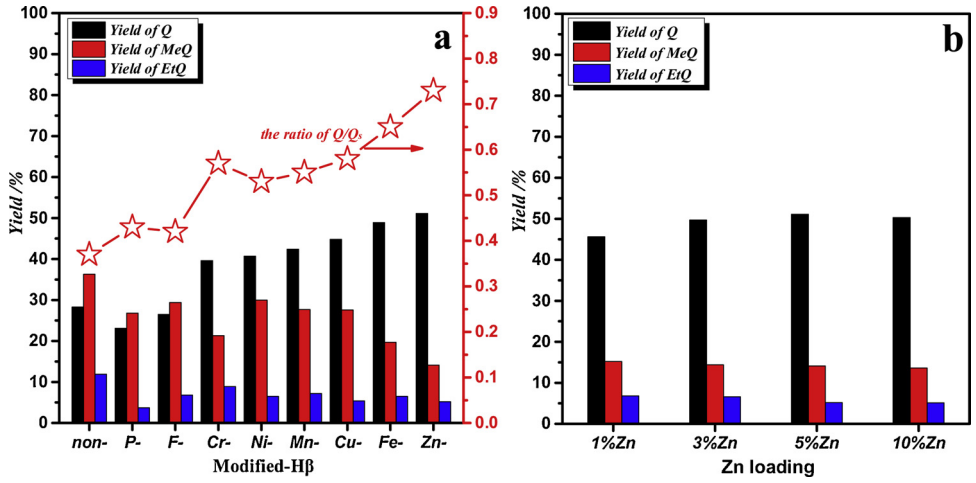

Fig. 1. The effect of modification and catalyst load of Hβ zeolite.

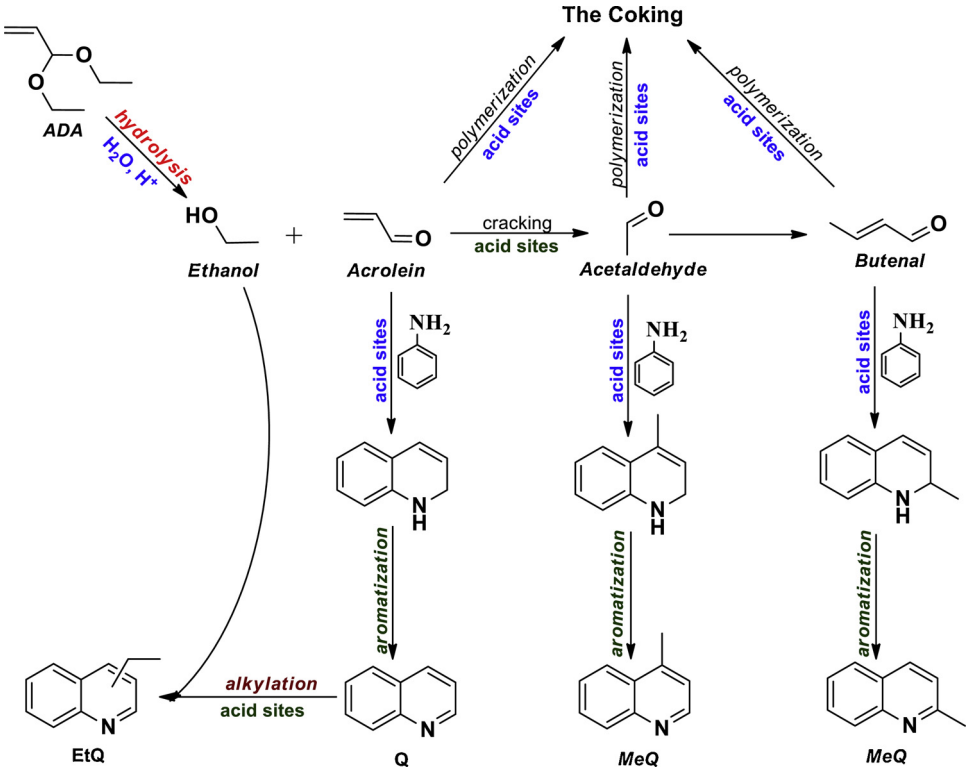

Scheme 1. Reaction routes in vapor-phase catalyzed acrolein diethyl acetal and aniline to quinolines over Hβ zeolite-base catalyst.

condensation-aromatization of acrolein/aniline to form Q [42]. Therefore, with increasing ratio of AN/ADA, the generated-acrolein is more easily to react with aniline to produce Q, whereas higher concentration of aniline maybe occupied acid sites excessively, restricting the reaction process to form Q.

(3) LHSV of mixture feedstocks. As shown in Fig. 2(c), with the increase of LHSV, yield of Q_s and Q increases, achieving the maximum values at the LHSV of 1.0 h^{-1} respectively, and then decreases. Residence time of reactants on the catalyst has a marked impact on the yield of quinolines. The reaction could be conducted more completely with a low value of LHSV, owning to prolong the residence time of reactants on the surface of catalyst. Whereas the long residence of intermediates on catalyst also result in the increasing of side reactions, such as, the polymeric-like reaction of acrolein, acetaldehyde and crotonaldehyde. On the contrary, the contact time of reactants and catalyst shortens with increasing the LHSV of feedstocks; as a result, the rapid leaving of the reactants from the catalyst surface leads to the relative conversion of reactants.

(4) LHSV of H_2O. As shown in Fig. 2(d), the addition of water to the reactor has significantly effect on the yield and selectivity of products. That not only promotes the hydrolysis of ADA to acrolein but also restrain the side-reactions (liking polymerization) via diluting concentration of active intermediates. However, excessively high value of LHSV of water could reduce the contacting probability of reactants; thereby, resulting in decreasing the formation of Q to some extent.

Fig. 3 shows the catalyst life of the Hβ and Zn/Hβ catalysts. With the increasing of reaction time, the yield of Q and Q_s decreases to different extent over Hβ and Zn/Hβ catalysts; whereas the trend of catalyst deactivation of Hβ catalyst declines slower than that of Zn/Hβ catalyst (Fig. 3a). The result reflects that the Zn/Hβ catalyst possesses better ability of anti-deactivation than the parent Hβ one. Besides, with increasing reaction time, the ratio of Q/Q_s decrease invariably over Hβ catalysts, but that of Q/Q_s initially decreases and appear to inverse at 9 h over Zn/Hβ one (Fig. 3b). This occurs probably due that the deposition of coking substances decreases pore size of the catalyst and then enhances diffusional limitation of quinolines products, thereby affecting the product's distribution.

Fig. 4 shows the regenerability of Zn/Hβ catalyst. The catalytic activity could almost completely recover by means of calcining at 550 C for 4 h in air. The result indicates that catalyst deactivation is reversible, mostly caused by the deposition of coking substances rather than devastating the structure of the catalyst. It is a remarkable fact that the life of the Zn/Hβ catalyst improves slightly compared to the Hβ one, although the regenerability of Zn/Hβ catalyst is excellent. This result reveals that the strong acid-induced polymerization of intermediates is not the crucial effect for the deactivation of catalyst. How to increase the life of the catalyst markedly is a great challenge and it is being investigated in our research group; for instance, an attractive strategy is to increase pore size of catalysts or prepare hierarchical structure catalyst.

3.2. Catalyst characterization

Fig. 5(a) shows the XRD patterns of Hβ and Zn/Hβ catalysts. Apparently, both of catalysts exhibit the typical characteristic of β zeolite. Especially, the Zn/Hβ catalyst don't appear the diffraction peaks of Zn species; which reflects that Zn species are highly dispersed on Hβ zeolite. Fig. 5(b) shows the FT-IR spectra of Hβ and Zn/Hβ catalysts. The Hβ and Zn/Hβ catalysts show the characteristic vibrations of BEA*-typed framework. It reported that the bands at ca. 1229 cm^{-1}, 1087 cm^{-1} and 797 cm^{-1} are assigned to the external asymmetric, internal asymmetric and external symmetric stretching vibrations of SiO_4/AlO_4 tetrahedron units [43–45], respectively. Meanwhile the bands at ca. 568 cm^{-1}, 524 cm^{-1} and 462 cm^{-1} are considered to be assigned to the typical β zeolite framework characteristic of double six-ring (D6R) and double four-ring (D4R) lattice vibrations of external linkage [46,47]. Besides, an extremely weak band at ca. 478 cm^{-1} is present over the Zn/Hβ catalyst but absent over the Hβ one, which

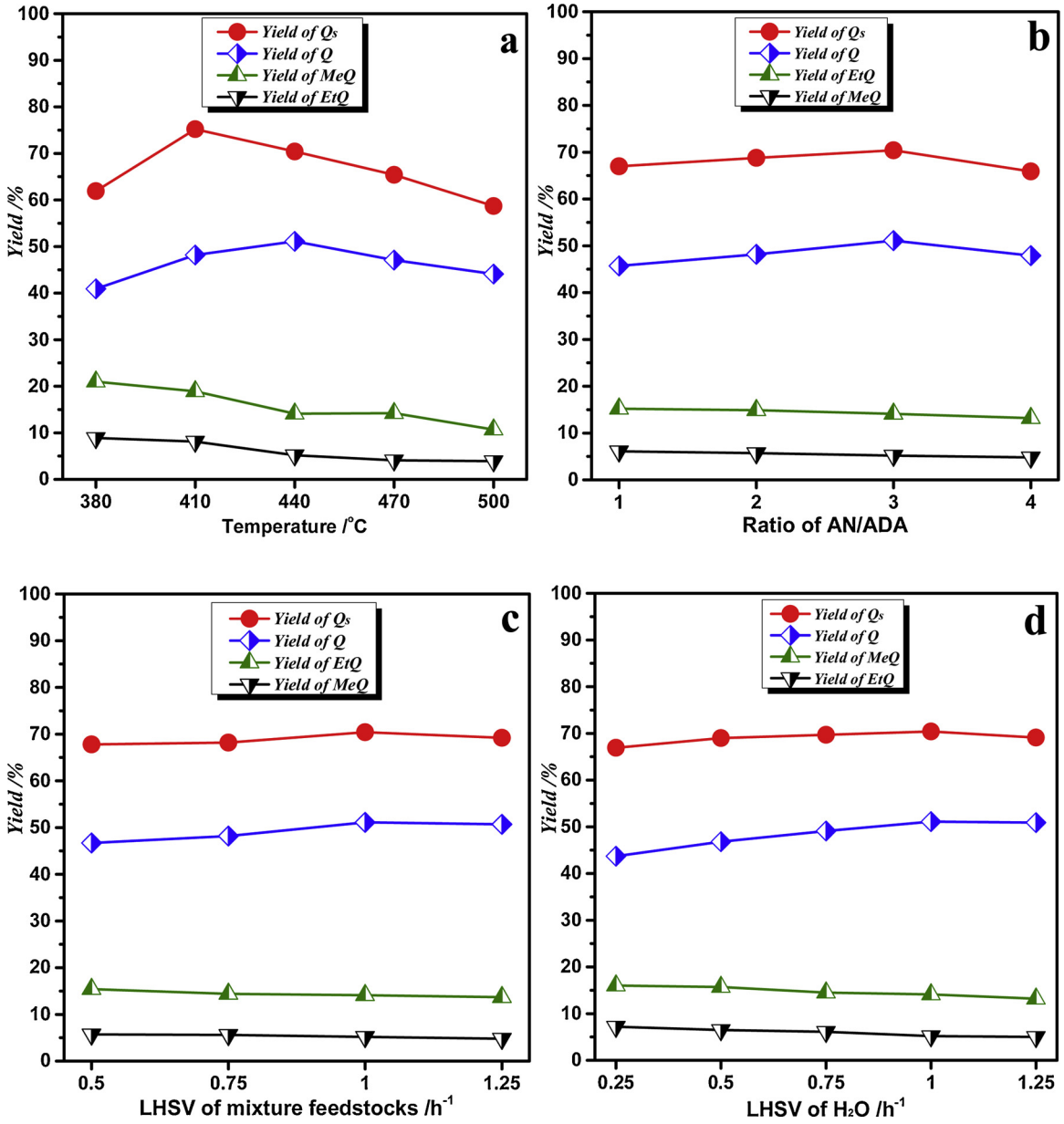

Fig. 2. The effect of reaction conditions over Zn/Hβ catalyst.

could be attributed to ZnO species [26]. The results further confirmed that the Hβ and Zn/Hβ catalysts possess well β zeolite framework structure, which is in agreement with the above XRD results.

Fig. 6 shows the SEM micrographs of Hβ and Zn/Hβ catalysts. Both of catalysts consist of many irregular bulk crystals with rough surfaces. Compared to the parent Hβ catalyst, the morphology and average size of crystals are no significant change over the Zn/Hβ one. Meanwhile, little bulky ZnO species could be seen on the surface of zeolite. Therefore, this SEM results indicate that the Zn-supported on zeolite have a negligible influence on morphology of the catalyst.

Fig. 7 shows the HRTEM micrographs of Hβ and Zn/Hβ catalysts. Compared to the Hβ catalysts, there is no distinctly contrast variation relating to the presence of ZnO particles notably different by mass density (Fig. 7c, d). It indicates that ZnO species are highly dispersed and not aggregated in a separate phase on the external surface of Hβ zeolite crystallites [40].

Fig. 8(a) shows the N_2 adsorption-desorption isotherms of Hβ and Zn/Hβ catalysts. A distinctly isotherms rise exists at exceedingly low relative pressure on Hβ and Zn/Hβ catalysts, mainly attributing to the N_2-adsorption in micropores. Meanwhile, a weak hysteresis loop at $P/P_0 > 0.4$ is present, reflecting that both of them exist certain mesopores. The existence of mesopores is most probably due to the aggregation of zeolite crystals to form intercrystal voids, which is manifested to be slitlike and irregular shape in the catalysts [48,49]. From the data of textural properties of catalysts (see Table 1), one can see that the Zn/Hβ catalyst possesses a smaller value of S_{BET}, S_{ext}, S_{mic}, V_{total}, V_{meso}, as well as V_{mic} and D_{mic}, relative to the Hβ one, mostly due to the dispersion of Zn species into micropore of zeolite.

Fig. 8(b) shows the NH_3-TPD profiles of Hβ and Zn/Hβ catalysts. The peak at ca. 159 °C occurs obviously over the Hβ and Zn/Hβ catalysts. Whereas the peak at ca. 495 °C appears distinctly over the Hβ one but disappears almost over the Zn/Hβ one. It reported that the peak of weak/medium acid sites of zeolites occurred at low temperature range (ca. 100 − 300 °C), whereas that of strong acid sites presented at high temperature range (ca. 300 − 500 °C) [50,51], which were assigned to the silanol groups at lattice defects or external surface and the proton of bridging Si-(OH)-Al groups of framework tetrahedral aluminum, respectively. From Table 2, one can see that the concentration of weak

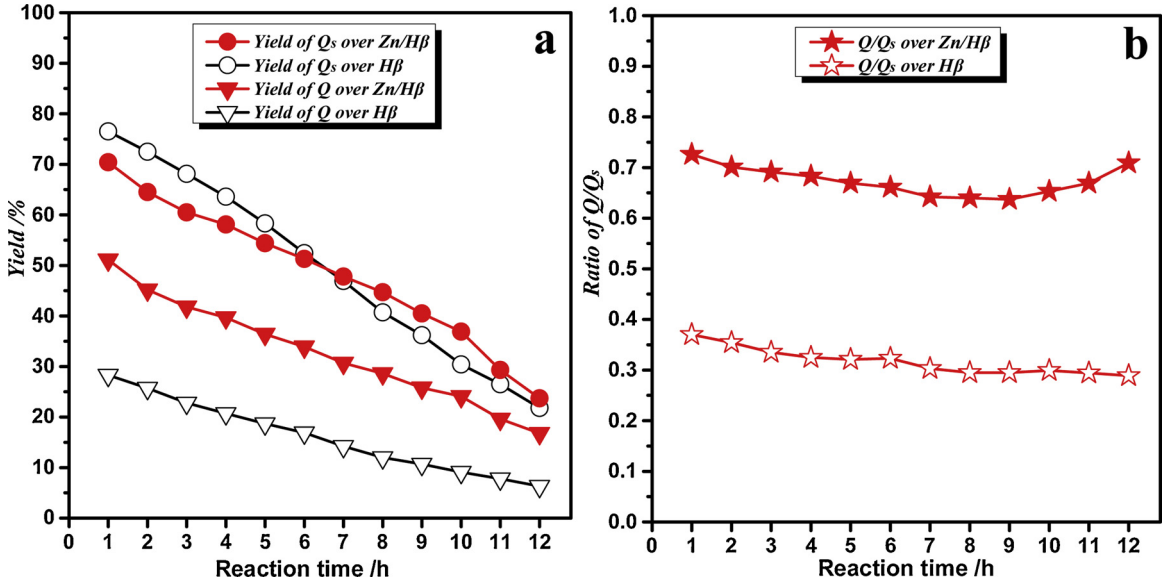

Fig. 3. The catalyst life of Zn/Hβ catalyst.

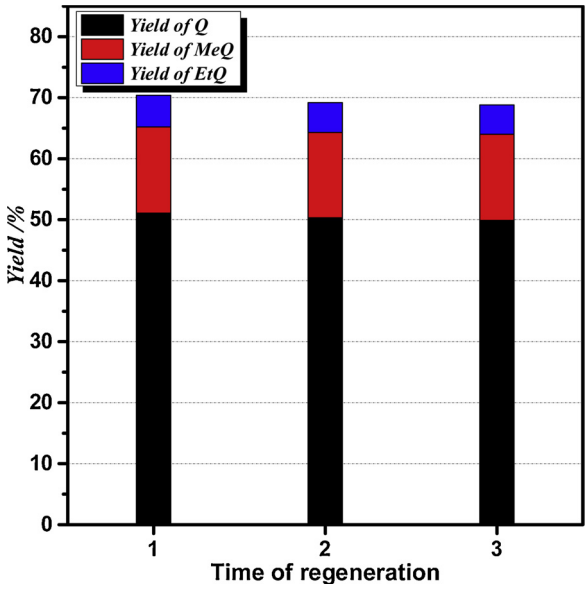

Fig. 4. The regenerability of Zn/Hβ catalyst.

acid decreases slightly but that of strong acid decreases sharply from 0.35 mmol/g to 0.07 mmol/g over the Zn/Hβ catalyst, compared to the parent Hβ one. This occurs due that the H^+ of bridging Si-(OH)-Al groups was exchanged by Zn^{2+} during the catalyst preparation process; thereby decreasing concentration of strong acid sites [31,32,52]. Therefore, the modification of Zn on zeolite regulates the concentration of acid sites of the catalyst effectively.

Fig. 9 shows the Zn $2p_{3/2}$ and Zn $2p_{1/2}$ XPS spectra for Zn/Hβ catalyst. For the bulk ZnO, the BE of Zn $2p_{3/2}$ and Zn $2p_{1/2}$ are at 1021.8–1022.5 eV and 1045.0 eV respectively [21]. Whereas that of Zn $2p_{3/2}$ are at 1022.4 eV and 1023.3 eV and that of Zn $2p_{1/2}$ is at 1045.9 eV over Zn/Hβ zeolite (Fig. 9), which is slightly shifted toward higher binding energy than those of bulk ZnO. The result indicates that the valence state of Zn species is most +2 over Zn/Hβ zeolite, most probably due to the stronger electronegativity group than O^{2-} group which leads to the higher BE [21]. Zhao et al. claimed that the BE of Zn $2p_{3/2}$ was 1022.16 eV if $ZnAl_2O_4$ crystallites was formed [53], indicating that there is no formation of $ZnAl_2O_4$ crystallites over the Zn/Hβ zeolite. This is probably due that the AlO_4 tetrahedrons in zeolite are very stable units and hard to interact with zinc species to form $ZnAl_2O_4$ crystallites. Furthermore, several literatures reported that the BE of Zn $2p_{3/2}$ of isolated O-$[Zn(OH)]^+$ species attached on various zeolites is at 1022.4–1023.0 eV, and that of isolated Zn^{2+} cations are inclined to shift toward higher binding energies, whereas that of Zn_nO_n clusters shift to lower binding energies of 1021.6–1022.2 eV with the BE value being lower for larger Zn_nO_n clusters [40,54,55]. For instance, Tamiyakul et al. demonstrated that the Zn species localized at the cation exchanged sites possess a high BE of about 1023.2 eV, due to its higher electronegativity of the lattice oxygen in zeolite than the O^{2-} ligand in bulk zinc oxide [54]. Gabrienko et al. concluded that the peak at BE 1022.8 eV for the ZnO/H-ZSM-5 could be reasonably assigned to -O-Zn-OH species as a part of ZnO clusters, which are a little bit larger than isolated O-$[Zn(OH)]^+$ species attached to the zeolite lattice [56]. Accordingly, the XPS result reveals that Zn/Hβ zeolite exists two state of zinc species, including both of isolated Zn^{2+} cations and ZnO clusters (-O-Zn-OH species); and meanwhile, it further implies that the Zn species is highly dispersed on the surface of zeolites.

The thermogravimetric profiles of the deactivated Hβ and Zn/Hβ catalysts are measured as shown in Fig. 10. The temperature in the range of 350 − 680 °C generally belongs to the burning of coking substances [31,57]. Apparently, the rate of weight loss of coking substances over Zn/Hβ catalyst is lower than that over Hβ one. The result indicates that the Zn/Hβ catalyst possesses relatively enhanced ability of anti-coking than the parent Hβ one, probably owing to the distinctly decreased concentration of strong acid site over the Zn/Hβ catalyst retarding the polymerization of reactive intermediates to form the coking.

3.3. Reaction mechanism

When the Zn/Hβ zeolite was used as catalysts in the synthesis of quinolines, Q was produced as the main product, and MeQ and EtQ were also generated in the product mixtures. Besides, the coking was formed in the reactor, indicating that the Zn/Hβ zeolite also catalyzed the polymerization reaction from different reactive intermediates. The reaction routes in vapor-phase ADA with aniline to quinolines over β zeolite-base catalyst are suggested as Scheme 1.

For the aza-heterocyclic-aromatization of ADA and aniline to Q, it suggested that ADA was firstly hydrolyzed to produce acrolein over acid sites [21], and then reacted with aniline to form dihydrogen quinoline via heterocyclization process. The resultant dihydrogenquinoline was

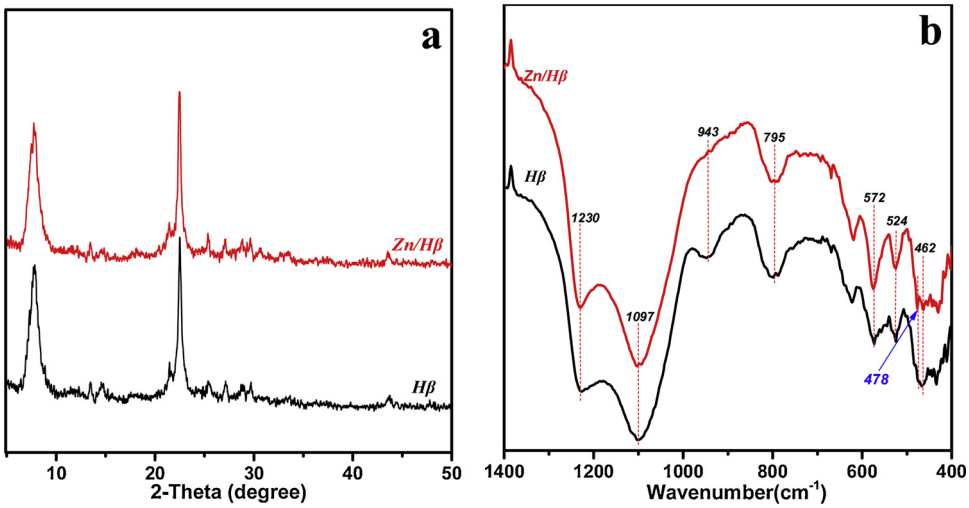

Fig. 5. The XRD patterns(a) and FT-IR spectra(b) for catalysts.

aromatized to generate Q via dehydrogenation process [11,34]. In our experiment, dihydrogenquinoline was detected from the product mixture with very low content, indicating that dihydrogenquinoline was dehydrogenated quickly to quinoline. MeQ and EtQ were also produced over the Zn/Hβ catalyst. It can be explained that MeQ was generated from the reaction between aniline and acetaldehyde under heterocyclization and aromatization processes; in which acetaldehyde derived from the cracking of acrolein [41,58]. 2-MeQ (2-methylquoniline) was produced through heterocyclization-aromatization processes of aniline with crotonaldehyde generated from condensation of acetaldehyde. Whereas 4-MeQ (4-methylquinoline) was generated from acetaldehyde directly reacting with aniline to form enamine, which subsequently reacts with another acetaldehyde to yield product via intramolecular electrophilic aromatic substitution [14,31]. In addition, EtQ were generated from the alkylation process of Q and ethanol which was the hydrolysis product of ADA over acid sites [35]. The formed coking in reactor was probably due to the acid-induced polymerization of intermediates involving acrolein, acetaldehyde as well as crotonaldehyde

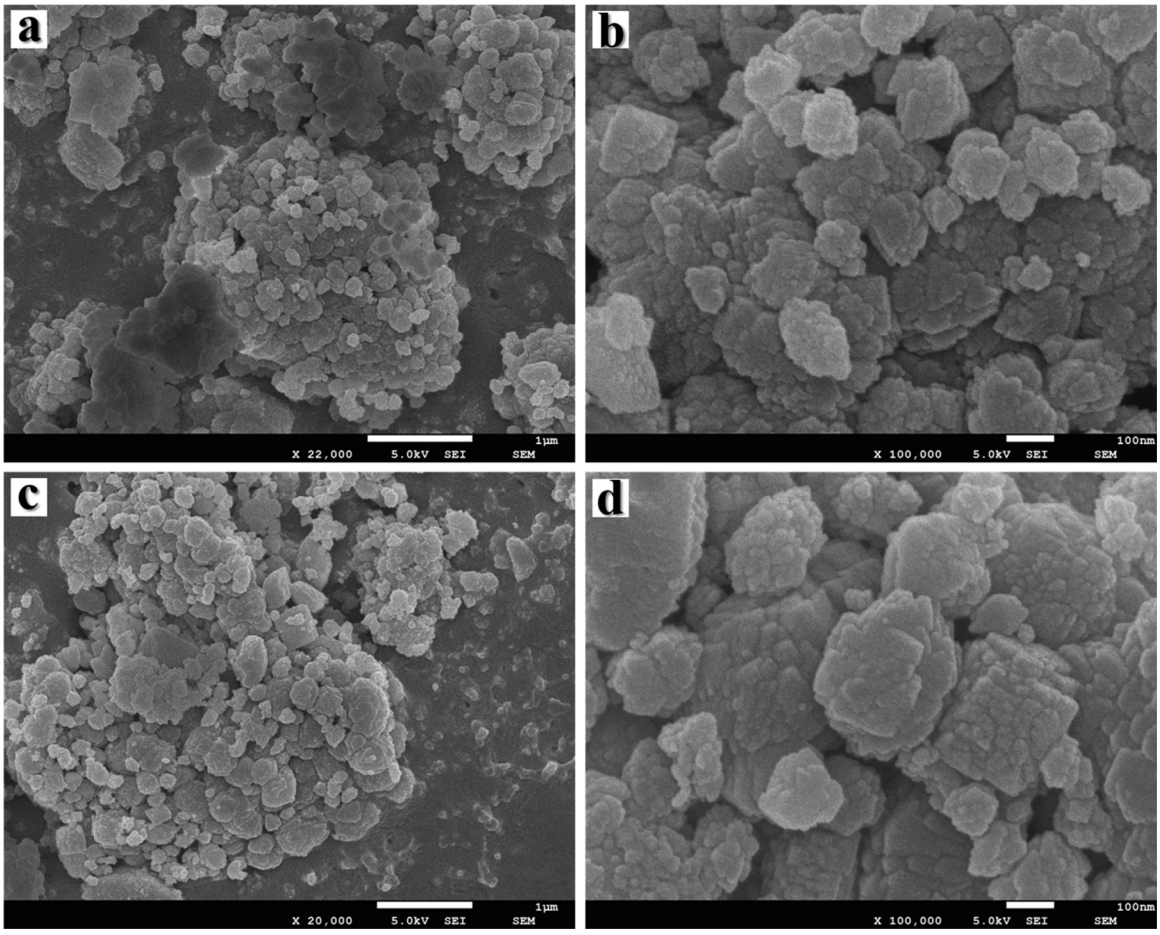

Fig. 6. The SEM images for Hβ(a, b) and Zn/Hβ(c, d) catalysts.

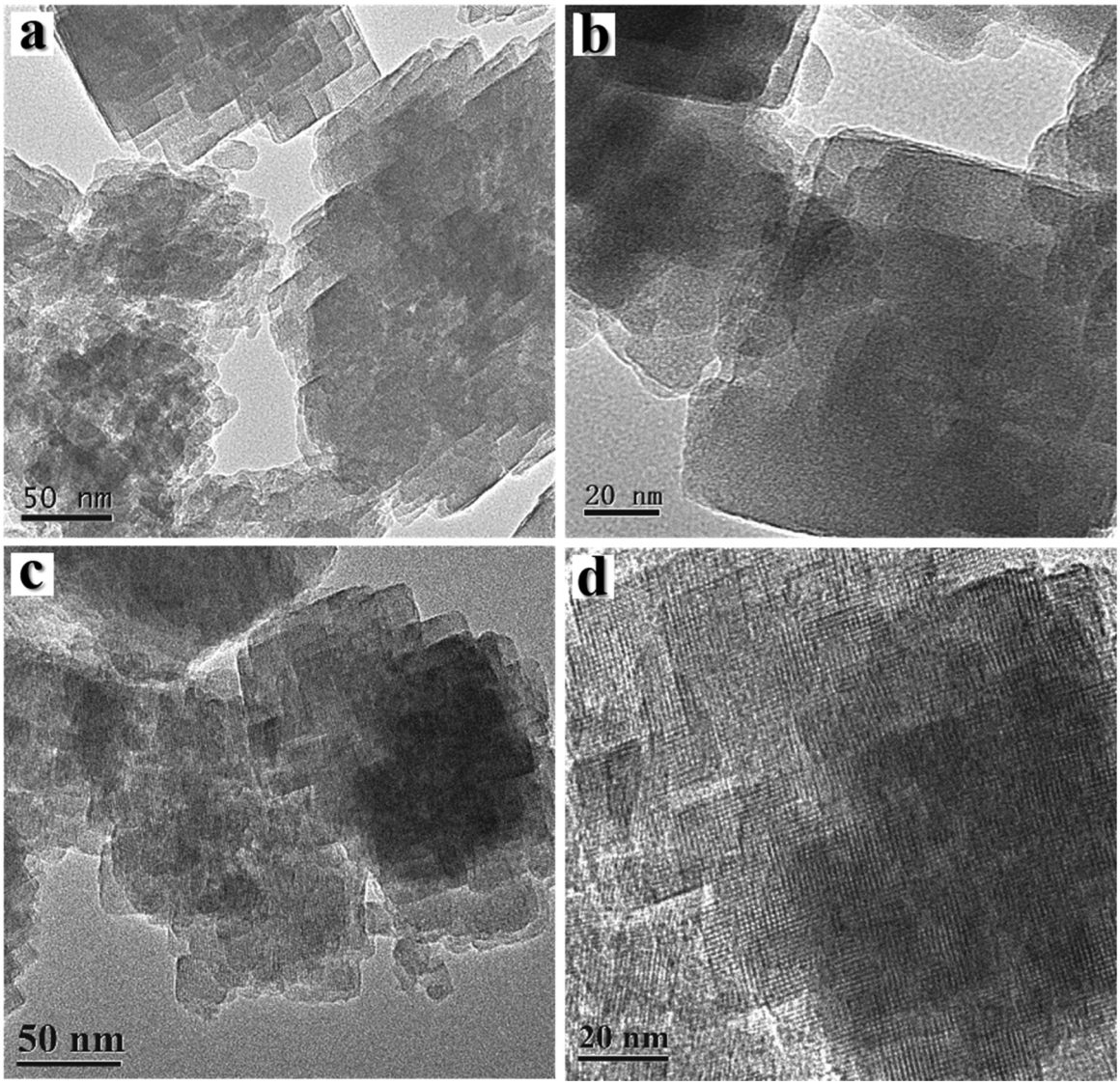

Fig. 7. The HRTEM images for Hβ(a, b) and Zn/Hβ(c, d) catalysts.

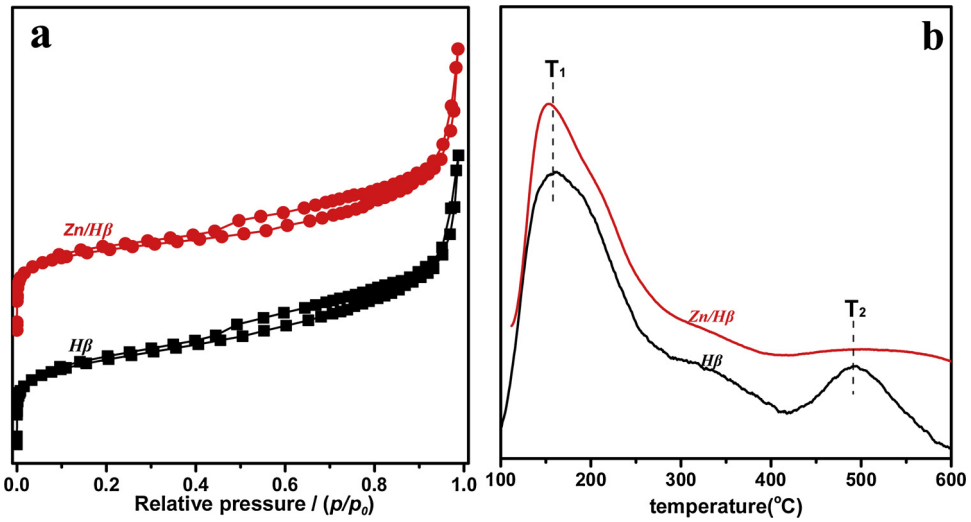

Fig. 8. The N_2 adsorption-desorption isotherms(a) and NH_3-TPD(b) for catalysts.

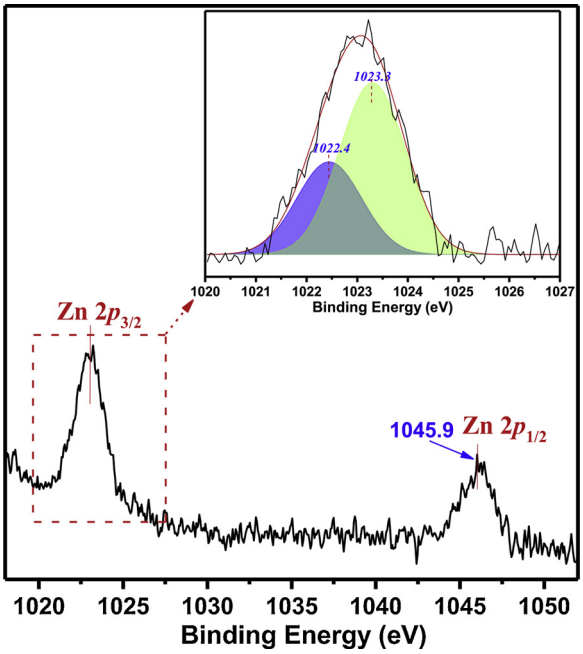

Fig. 9. The Zn $2p_{3/2}$ and Zn $2p_{1/2}$ XPS spectra for Zn/Hβ catalyst.

Table 1
The textural properties for Hβ and Zn/Hβ catalysts.

Catalyst	S_{BET} (m^2/g)	S_{ext} (m^2/g)	S_{mic} (m^2/g)	V_{total} (cm^3/g)	V_{mic} (cm^3/g)	V_{meso} (cm^3/g)	D_{mic} (nm)
Hβ	483.7	168.2	315.5	0.40	0.15	0.25	0.60
Zn/Hβ	443.3	147.9	295.4	0.38	0.14	0.24	0.59

S_{BET}, S_{ext} and S_{mic} refers to specific surface area, external surface area and micropore surface area, respectively, and $S_{BET} = S_{ext} + S_{mic}$; Vt_{total} and V_{mic} refers to total pore volume and micropore volume, respectively. D_{mic} refers to the micropore diameter calculated via SF method.

Table 2
The NH_3-TPD results for Hβ and Zn/Hβ catalysts.

Catalyst	T_i [a] (°C) and A_i [b] (mmol/g) for various desorption peaks				
	T_1	A_1	T_2	A_2	A_{total}
Hβ	159.6	1.23	494.5	0.35	1.58
Zn/Hβ	159.6	1.22	494.5	0.07	1.29

[a] T_i refers to the temperature at the maximum of desorption peak i.
[b] A_i refers to the integral area of desorption peak i, and it means also the concentration of acid site corresponding to the desorption peak i; A_{total} stands for the sum of the concentration of various acid site, i.e., $A_{total} = \Sigma A_i$.

[41].

Compared to the parent Hβ zeolite catalyst, the yield of Q increases distinctly while that of MeQ and EtQ declined apparently over the Zn/Hβ zeolite one. The results indicate that the modified of Zn species on zeolites significantly affect the distribution of quinolines products. It reported that strong acid sites on catalysts not only accelerated the cracking process of hydrocarbon compounds but also favored the alkylation reaction at relatively high temperature [32,35]. On account of the addition of Zn species on Hβ zeolites decreasing the concentration of strong acid sites of the catalyst, the Zn/Hβ zeolite catalyst could restrain the cracking of acrolein to acetaldehyde as well as the alkylation of Q to EtQ. Moreover, highly dispersed ZnO clusters over Zn/Hβ catalyst could enhance aromatization process of dihydroquinoline to quinoline. As a result, higher yield of Q obtained over the Zn/Hβ catalyst than the parent Hβ one. Besides, strong acid sites easily induce the

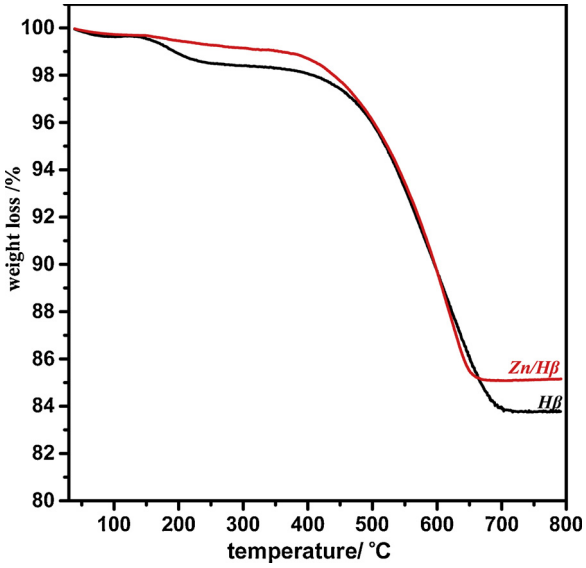

Fig. 10. The TG profiles of the deactivated Hβ and Zn/Hβ catalysts.

polymerization of aldehydes/ketones to form coking; therefore, the Zn/Hβ catalyst possessed the better ability of anti-deactivation than the Hβ one.

Besides, the comparison of different reagents reacting with aniline to vapor-phase generate quinoline was listed in table 2S. Compared to using allyl alcohol, acrolein or aldehydes as raw materials, higher yield of quinoline could be obtained when using ADA as raw material. When using glycerol as feedstock, the brilliant yield of quinoline has been achieved, whereas catalyst was easier to be deactivated. Therefore, according to high yield of quinolines as well as the desired regeneration of catalyst, this vapor-phase route developed in this work, co-employing Zn/Hβ as green and mild catalyst, presents the potential importance of industrial manufacture.

4. . Conclusions

A sustainable approach for gas-phase catalyzed aza-heterocyclic-aromatization of acrolein dimethyl acetal and aniline to quinolines was successfully developed in this work, utilizing Zn-modified Hβ zeolites as environmental-friendly catalysts. Quinoline, methylquinolines and ethylquinolines were generated in this reaction. The modified of Zn on zeolites significantly affected the distribution of quinolines products, because the Zn^{2+} cations together with dispersed ZnO clusters over Zn/Hβ catalyst not only decreased concentration of strong acid sites but also enhanced enhance aromatization process of dihydroquinoline to quinoline. As a result, the Zn/Hβ catalyst possessed better selectivity of quinoline than the parent Hβ one, owing to the decrease of concentration of strong acid sites restraining the cracking of acrolein to acetaldehyde as well as the alkylation of quinoline to ethylquinoline. Reaction influence factors were also systematically evaluated. Under the optimized operating conditions, e.g. Temperature = 440 °C, ratio of AN/ADA = 3:1, LHSV of mixture feedstocks = 1.0 h^{-1}, LHSV of H_2O = 1.0 h^{-1}, more than 51 % yield of quinoline were obtained over Zn/Hβ catalyst; which far exceeded the yield of quinoline over the pure Hβ one. The Zn/Hβ catalyst showed relatively enhanced anti-deactivated performance and excellent regenerability, due to decrease acid-induced polymerization of active intermediates to form the coking. Besides, a plausible reaction routes in vapor-phase acrolein diethyl acetal with aniline to yield quinoline, methylquinoline and ethylquinoline was suggested in this paper.

CRediT authorship contribution statement

An Li: Conceptualization, Methodology, Investigation, Writing - original draft. **Caiwu Luo:** Writing - review & editing, Validation, Formal analysis, Visualization. **Yong Liu:** Validation, Formal analysis, Visualization. **Lijun Li:** Writing - review & editing, Supervision. **Ying Lin:** Data curation, Resources. **Kun Liu:** Conceptualization, Methodology, Writing - review & editing. **Congshan Zhou:** Conceptualization, Methodology, Writing - review & editing.

Declaration of Competing Interest

The authors declare that they have no known competing financial interests or personal relationships that could have appeared to influence the work reported in this paper.

Acknowledgments

This work was supported by the National Natural Science Foundation of China (No. 51978648), the Hunan Provincial Natural Science Foundation of China (No. 2019JJ50215), the Joint Funds of Hunan Province Engineering Research Center of Radioactive Control Technology in Uranium Mining and Metallurgy & Hunan Province Engineering Technology Research Center of Uranium Tailings Treatment Technology (2019YKZX2012), the Opening Project of Cooperative Innovation Center for Nuclear Fuel Cycle Technology and Equipment, University of South China (2019KFQ18).

Appendix A. Supplementary data

Supplementary material related to this article can be found, in the online version, at doi:https://doi.org/10.1016/j.mcat.2020.110833.

References

[1] N.H. Lin, P. Xia, P. Kovar, C. Park, Z. Chen, H. Zhang, S.H. Rosenberg, H.L. Sham, Bioorg. Med. Chem. Lett. 16 (2006) 421–426.
[2] N. Mahindroo, C.C. Wang, C.C. Liao, C.F. Huang, I.L. Lu, T.W. Lien, Y.H. Peng, W.J. Huang, Y.T. Lin, M.C. Hsu, C.H. Lin, C.H. Tsai, J.T.A. Hsu, X. Chen, P.C. Lyu, Y.S. Chao, S.Y. Wu, H.P. Hsieh, J. Med. Chem. 49 (2006) 1212–1216.
[3] I. Bolea, J. Juárez-Jiménez, C. de los Ríos, M. Chioua, R. Pouplana, F.J. Luque, M. Unzeta, J. Marco-Contelles, A. Samadi, J. Med. Chem. 54 (2011) 8251–8270.
[4] M.P. Pinz, A.S. dos Reis, A.G. Vogt, R. Krüger, D. Alves, C.R. Jesse, S.S. Roman, M.P. Soares, E.A. Wilhelm, C. Luchese, Biomed. Pharmacother. 105 (2018) 1006–1014.
[5] P. Shah, D. Naik, N. Jariwala, D. Bhadane, S. Kumar, S. Kulkarni, K.K. Bhutani, I.P. Singh, Bioorg. Chem. 80 (2018) 591–601.
[6] A. Corma, A. Leyva-Pérez, M.J. Sabater, Chem. Rev. 111 (2011) 1657–1712.
[7] E. Pérez Mayoral, E. Soriano, V. Calvino-Casilda, M.L. Rojas-Cervantes, R.M. Martín-Aranda, Catal. Today 285 (2017) 65–88.
[8] C.M. Leir, J. Org. Chem. 42 (1977) 911–913.
[9] W.P. Utermohlen,, J. Org, Chem. 08 (1943) 544–549.
[10] B. Zhang, A. Studer, Chem. Soc. Rev. 44 (2015) 3505–3521.
[11] G.A. Ramann, B.J. Cowen, Tetrahedron Lett. 56 (2015) 6436–6439.
[12] Y. Kobayashi, J. Igarashi, C. Feng, Tojo Toshifumi, Tetrahedron Lett. 53 (2012) 3742–3745.
[13] C.M. Leir, J. Org. Chem. 42 (1977) 911.
[14] R. Brosius, D. Gammon, F. Vanlaar, E. Vansteen, B. Sels, P. Jacobs, J. Catal. 239 (2006) 362–368.
[15] J.R. Calvin, R.D. Davis, C.H. McAteer, Appl. Catal. A Gen. 285 (2005) 1–23.
[16] B.M. Reddy, I. Ganesh, J. Mol. Catal. A Chem. 151 (2000) 289–293.
[17] M. Campanatia, A. Vaccari, O. Piccolo, Catal. Today 60 (2000) 289–295.
[18] Y. Wang, S. Furukawa, X. Fu, N. Yan, ACS Catal. 10 (2020) 311–335.
[19] Ma.R. Capeletti, L. Balzano, G. de la Puente, M. Laborde, U. Sedran, Appl. Catal. A Gen. 198 (2000) 1–4.
[20] J. Deutsch, A. Martin, H. Lieske, J. Catal. 245 (2007) 428–435.
[21] C.W. Luo, A. Li, J.F. An, X.Y. Feng, X. Zhang, D.D. Feng, Z.S. Chao, Chem. Eng. J. 273 (2015) 7–18.
[22] A. Musˇicˇ, J. Batista, J. Levec, Appl. Catal. A Gen. 165 (1997) 115–131.
[23] Z. Liu, Z. Liu, T. Cui, J. Li, J. Zhang, T. Chen, X. Wang, X. Liang, Chem. Eng. J. 235 (2014) 257–263.
[24] A. Nezamzadeh-Ejhieh, S. Khorsandi, J. Ind. Eng. Chem. 20 (2014) 937–946.
[25] S. Anandan, A. Vinu, N. Venkatachalam, B. Arabindoo, V. Murugesan, J. Mol. Catal. A Chem. 256 (2006) 312–320.
[26] W. Lu, G. Lu, Y. Luo, A. Chen, J. Mol. Catal. A Chem. 188 (2002) 225–231.
[27] C. Chen, Z. Hu, J. Ren, S. Zhang, Z. Wang, Z.Y. Yuan, ChemCatChem 11 (2019) 868–877.
[28] N. Wang, W. Qian, K. Shen, C. Su, F. Wei, Chem. Commun. 52 (2016) 2011–2014.
[29] H. Chen, T. Chen, K. Chen, J. Fu, X. Lu, P. Ouyang, Catal. Commun. 103 (2018) 38–41.
[30] J. Heemsoth, E. Tegeler, F. Roessner, A. Hagen, Microporous Mesoporous Mater. 46 (2001) 185–190.
[31] A. Li, C. Huang, C.W. Luo, W.J. Yi, Z.S. Chao, RSC Adv. 7 (2017) 9551–9561.
[32] A. Li, C. Huang, C.W. Luo, L.J. Li, W.J. Yi, T.W. Liu, Z.S. Chao, Catal. Commun. 98 (2017) 13–16.
[33] M. Campanati, P. Savini, A. Tagliani, A. Vaccari, Catal. Lett. 47 (1997) 247–250.
[34] S. Kamiguchi, I. Takahashi, H. Kurokawa, H. Miura, T. Chihara, Appl. Catal. A Gen. 309 (2006) 70–75.
[35] P.R. Reddy, K.V.S. Rao, M. Subrahmanyam, Catal. Lett. 56 (1998) 155–158.
[36] J.C. Jansen, E.J. Creyghton, S.L. Njo, Hv. Koningsveld, Hv. Bekkum, Catal. Today 38 (1997) 205–212.
[37] H. Yang, P. Yang, X. Liu, Y. Wang, Chem. Eng. J. 299 (2016) 112–119.
[38] S.M.G. Majano, O. Ovsitser, T.B.B. Mihailova, Microporous Mesoporous Mater. 80 (2005) 227–235.
[39] C. McAteer, R.D. Sr, J. Calvin, US Patent, 5700942 (1997).
[40] A.A. Gabrienko, S.S. Arzumanov, A.V. Toktarev, I.G. Danilova, I.P. Prosvirin, V.V. Kriventsov, V.I. Zaikovskii, D. Freude, A.G. Stepanov, ACS Catal. 7 (2017) 1818–1830.
[41] L. Shen, H. Yin, A. Wang, Y. Feng, Y. Shen, Z. Wu, T. Jiang, Chem. Eng. J. 180 (2012) 277–283.
[42] B.M. Reddy, I. Ganesh, J. Mol. Catal. A Chem. 151 (2000) 289–293.
[43] A. Vimont, F. Thibault-Starzyk, J.C. Lavalley, J. Phys. Chem. B 104 (2000) 286–291.
[44] I. Othman, R.M. Mohamed, I.A. Ibrahim, M.M. Mohamed, Appl. Catal. A Gen. 299 (2006) 95–102.
[45] L. Shirazi, E. Jamshidi, M.R. Ghasemi, Cryst. Res. Technol. 43 (2008) 1300–1306.
[46] J. Perez-Pariente, J.A. Martens, P.A. Jacobs, Appl. Catal. 31 (1987) 35–64.
[47] I. Kiricsi, C. Flego, G. Pazzuconi, W.O. Parker Jr, R. Millini, C. Perego, G. Bellussi, J. Phys. Chem. 98 (1994) 4627–4634.
[48] T. Armaroli, L.J. Simon, M. Digne, T. Montanari, M. Bevilacqua, V. Valtchev, J. Patarin, G. Busca, Appl. Catal. A Gen. 306 (2006) 78–84.
[49] C.W. Luo, C. Huang, A. Li, W.J. Yi, X.Y. Feng, Z.J. Xu, Z.S. Chao, Ind. Eng. Chem. Res. 55 (2016) 893–911.
[50] Y.T. Kim, K.D. Jung, E.D. Park, Microporous Mesoporous Mater. 131 (2010) 28–36.
[51] B.O.D. Costa, M.A. Peralta, C.A. Querini, Appl. Catal. A Gen. 472 (2014) 53–63.
[52] B.L. Su, V. Norberg, Zeolites 19 (1997) 65–74.
[53] Y. Zhang, T. Wei, Y. Pian, J. Zhao, Appl. Catal. A Gen. 467 (2013) 154–162.
[54] S. Tamiyakul, W. Ubolcharoen, D.N. Tungasmita, S. Jongpatiwut, Catal. Today 256 (2015) 325–335.
[55] T. Gong, L. Qin, J. Lu, H. Feng, Phys. Chem. Chem. Phys. 18 (2016) 601–614.
[56] J.F. Moudler, W.F. Stickle, W.T. Sobol, K.D. Bomben, Handbook of X-ray Photoelectron Spectroscopy, (1992).
[57] C.W. Luo, Z.S. Chao, RSC Adv. 5 (2015) 54090–54101.
[58] E. Tsukuda, S. Sato, R. Takahashi, T. Sodesawa, Catal. Commun. 8 (2007) 1349–1353.